TIA1 potentiates tau phase separation and promotes generation of toxic oligomeric tau

Peter E. A. Ash[a,1], Shuwen Lei[a,1], Jenifer Shattuck[a], Samantha Boudeau[a], Yari Carlomagno[b], Maria Medalla[c,d], Bryce L. Mashimo[a], Guillermo Socorro[a], Louloua F. A. Al-Mohanna[a], Lulu Jiang[a], Muhammet M. Öztürk[a], Mark Knobel[a], Pavel Ivanov[e], Leonard Petrucelli[b], Susanne Wegmann[f], Nicholas M. Kanaan[g], and Benjamin Wolozin[a,d,h,i,2]

[a]Department of Pharmacology and Experimental Therapeutics, Boston University School of Medicine, Boston, MA 02118; [b]Department of Neuroscience, Mayo Clinic Florida, Jacksonville, FL 32224; [c]Department of Anatomy and Neurobiology, Boston University School of Medicine, Boston, MA 02118; [d]Department of Neurology, Boston University School of Medicine, Boston, MA 02118; [e]Division of Rheumatology, Immunology, and Allergy, Brigham and Women's Hospital, Harvard Medical School, Boston, MA 02115; [f]German Center for Neurodegenerative Diseases, DZNE, Berlin, 10117, Germany; [g]Department of Translational Neuroscience, Grand Rapids Research Center, Michigan State University, Grand Rapids, MI 49503; [h]Center for Systems Neuroscience, Boston University School of Medicine, Boston, MA 02118; and [i]Neurophotonics Center, Boston University School of Medicine, Boston, MA 02118

Edited by Gregory A. Petsko, Brigham and Women's Hospital, Boston, Massachusetts, and approved January 19, 2021 (received for review July 7, 2020)

Tau protein plays an important role in the biology of stress granules and in the stress response of neurons, but the nature of these biochemical interactions is not known. Here we show that the interaction of tau with RNA and the RNA binding protein TIA1 is sufficient to drive phase separation of tau at physiological concentrations, without the requirement for artificial crowding agents such as polyethylene glycol (PEG). We further show that phase separation of tau in the presence of RNA and TIA1 generates abundant tau oligomers. Prior studies indicate that recombinant tau readily forms oligomers and fibrils in vitro in the presence of polyanionic agents, including RNA, but the resulting tau aggregates are not particularly toxic. We discover that tau oligomers generated during copartitioning with TIA1 are significantly more toxic than tau aggregates generated by incubation with RNA alone or phase-separated tau complexes generated by incubation with artificial crowding agents. This pathway identifies a potentially important source for generation of toxic tau oligomers in tau-related neurodegenerative diseases. Our results also reveal a general principle that phase-separated RBP droplets provide a vehicle for coassortment of selected proteins. Tau selectively copartitions with TIA1 under physiological conditions, emphasizing the importance of TIA1 for tau biology. Other RBPs, such as G3BP1, are able to copartition with tau, but this happens only in the presence of crowding agents. This type of selective mixing might provide a basis through which membraneless organelles bring together functionally relevant proteins to promote particular biological activities.

oligomeric tau | fibrillar tau | liquid–liquid phase separation (LLPS) | Alzheimer's disease | RNA binding proteins

A characteristic of progressive neurodegenerative tauopathies is the accumulation of insoluble neurofibrillary tangles (NFTs) composed of hyperphosphorylated fibrillar tau protein (f.tau) (microtubule-associated protein tau [MAPT]) in affected neurons (1). Fibrillization can be recapitulated in vitro by mixing recombinant human tau with polyanionic compounds such as heparin, arachidonic acid, or RNA (2, 3). Through nonspecific electrostatic interaction with the tau repeat domain, RNA may function as a physiological inducer of tau fibrillization (4, 5). However, f.tau does not appear to be the primary neurotoxic driver of toxicity in tauopathies (6, 7). Mounting evidence suggests that toxicity mainly arises from oligomeric tau (o.tau) species (8–11), which are thought to be temporal intermediate tau units in the polymerization of f.tau (12, 13).

Phase separation has emerged as a fundamentally important process in biology (14, 15). Nonmembrane bound protein condensates form in response to cellular signals and allow for dynamic compartmentalization of biomolecules for the completion of defined biochemical reactions. Recently, tau was shown to undergo liquid–liquid phase separation (LLPS) in the presence of molecular crowding agents (16). The low sequence complexity of tau generates intrinsically disordered regions (IDRs), which are characteristic of proteins that undergo phase separation (17, 18). Initially, phase separation produces droplets of dynamic liquid tau (l.tau) that with time gelates into vitrified tau (v.tau) (19). Condensates of tau may be a necessary stage in recruiting and concentrating tubulin (~10-fold higher than outside tau droplets) for the purpose of nucleating microtubules (16). Tau also coacervates with RNA into liquid droplets in vitro (20, 21) and with RNA binding proteins (RBPs) in cells in response to stress (22, 23). More recent work showed that PEG-induced LLPS can generate tau oligomers involving N-terminal exposure in the absence of fibril formation (24). However, prior work leaves unknown whether phase separation induced by RNA or RBPs plays a role in tau pathology and tau toxicity. In Alzheimer's disease (AD) models, tau interacts with RBPs in a manner that induces pathogenic alterations to tau (25, 26).

Significance

Phase separation of proteins is increasingly thought to play a fundamental role in biological processes. Recent studies show that tau protein phase separates, but the biological significance is unknown since artificial crowding agents are typically used and the resulting tau is not toxic. We now demonstrate that TIA1 potentiates RNA-mediated phase separation of tau, thereby enabling a process that occurs at physiological concentrations and also directs the formation of biologically active, highly neurotoxic oligomeric tau. Coordinated phase separation of functionally related proteins provides a general mechanism through which membraneless organelles can direct biological activities.

Author contributions: P.E.A.A. and B.W. designed research; P.E.A.A., S.L., J.S., S.B., M.M., B.L.M., G.S., L.F.A.A.-M., L.J., M.M.Ö., and P.I. performed research; P.E.A.A., S.L., J.S., Y.C., P.I., L.P., S.W., N.M.K., and B.W. contributed new reagents/analytic tools; P.E.A.A., S.L., M.K., and B.W. analyzed data; and P.E.A.A. and B.W. wrote the paper.

Competing interest statement: B.W. is co-founder and chief scientific officer for Aquinnah Pharmaceuticals, Inc.

This article is a PNAS Direct Submission.

[1]P.E.A.A. and S.L. contributed equally to this work.

[2]To whom correspondence may be addressed. Email: bwolozin@bu.edu.

This article contains supporting information online at https://www.pnas.org/lookup/suppl/doi:10.1073/pnas.2014188118/-/DCSupplemental.

Published February 22, 2021.

Interaction of tau with TIA1, a stress granule (SG) nucleating RBP (27), is necessary for tau-dependent neurodegeneration in PS19 transgenic mice (8). Survival of and behavioral deficits in tau transgenic mice correlated with levels of TIA1-dependent oligomeric tau. We subsequently showed that TIA1 is required for the propagation of oligomeric tau (but not fibrillar tau) across the brains of young PS19 mice, resulting in o.tau-dependent neurodegeneration (9). This raises the possibility that interaction with RBPs facilitates the phase separation of tau and the production of toxic tau species.

The kinetics of phase separation are governed by determinants that affect intermolecular interactions (28) and the sufficient availability of interaction sites (a biomolecule's "valence") on each particle within a connected system (29). For RBPs (and tau), phase separation is dependent on temperature, pH, and on concentration of RNA, salt, and crowding agent following the Flory–Huggins theory of polymer solutions (30, 31). This theory describes the combined energetics of protein–protein, RNA–RNA, protein–RNA, protein–solute, and RNA–solute interactions within the system. As such, phase separation occurs when homo- and heterogeneous molecular interactions between tau and other biomolecules (such as RNA) offer sufficient gain in enthalpy to surmount the loss of system entropy.

Here we show an essential role for RBPs in directing tau phase separation and the type of tau pathology that accumulates. In the presence of RNA and the RNA binding protein TIA1, phase separation of tau occurs at physiological concentrations. Furthermore, TIA1 blocks the RNA-dependent conversion of o.tau into f.tau in vitro, leading to accumulation of neurotoxic o.tau species. Our data strongly suggest that direct interaction with TIA1 promotes phase separation of tau and regulates the formation of toxic oligomeric tau.

Results

Microtubule Binding Domain Interaction with RNA Drives Phase Separation of Tau. Physiological LLPS of tau may depend on coacervation of tau with RNA in a crowded cellular environment (20). We sought to understand the structural components of tau that drive RNA-induced phase separation in the presence or absence of the molecular crowding agent polyethylene glycol (PEG). Crowding agents can induce protein LLPS by increasing the local protein concentration through excluded volume effects, thereby mimicking the molecular crowding that occurs in the cell (32). Within such a system, the crowding agent limits the degrees of freedom experienced by protein and RNA components, thereby increasing stochastic molecular collision (leading to formation of droplets) and promoting the recruitment of protein into existing droplets (increasing the mean area of droplets).

We induced phase separation of 5 μM recombinant human 0N4R tau conjugated with DyLight-488 (tau-488) using 10% PEG (PEG-8000) (Fig. 1*A*). LLPS reactions were incubated for 2 h before imaging droplets by differential interference contrast (DIC) and fluorescent microscopy. Fluorescent images were then exported for quantification of droplets as percent coverage of field of view (FOV), particle number, and particle size. Phase separation of tau-488 responds to concentration of NaCl and RNA in a nonlinear fashion (*SI Appendix*, Fig. S1 *A–C*). Maximal phase separation occurred at 50 mM NaCl and 60 ng/μL RNA. Within the range of ∼50 mM NaCl and 40 to 60 ng/μL total murine brain RNA, tau–tau, and tau–RNA interactions are dominant leading to demixing. Inefficient LLPS occurs with 1) too little NaCl (<25 mM) or too little RNA (<20 ng/μL) leading to unfavorable tau–RNA and tau–tau interactions; 2) too much NaCl (>100 mM) where tau–solute and RNA–solute interactions are dominant; or 3) too much RNA (>70 ng/μL) leading to RNA–solute dominant interactions.

Next, we examined the role of tau domains in promoting tau LLPS. Using recombinant domains of tau conjugated with DyLight-488 (amino acid [aa] numbering according to the largest 2N4R tau isoform having 441 aa, Fig. 1 *B*, *i*), we quantified phase separation as percentage coverage of FOV and as number of droplets formed (Fig. 1 *E* and *F*). Assessing which domains of tau undergo LLPS (green bars in Fig. 1 *B*, *ii*) and which do not (blue bars in Fig. 1 *B*, *ii*), allowed identification of tau domains that contribute to LLPS of the full-length protein (highlighted green in Fig. 1 *B*, *iii*).

In the presence of 20 ng/μL RNA and 10% PEG, droplets were robustly formed from 0N4R tau, the projection domain (aa 9 to 155), the first proline-rich domain (P1, aa 163 to 209), the microtubule binding domain (MTBD, repeats R1, R2, R3, and R4, aa 225 to 380), and the C-terminal end (aa 344 to 441, including R4 and C-terminal end) (Fig. 1*C*). Interestingly, MTBD-488 droplets induced by the presence of PEG + RNA appeared to be nonhomogenous, perhaps suggesting regions of reduced fluidity are forming (Fig. 1*C*, arrows). No droplets were formed from the N-terminal domain (aa 1 to 224, including N1 and N2), the central portion (aa 144 to 273, including proline-rich domains P1, and P2, and R1), and the N-terminally extended MTBD (aa 209 to 356, including P2 and most of the MTBD). The suppression of MTBD LLPS by P2 in the aa 209 to 356 construct suggests that the P2 domain may engage in intermolecular and solute interactions that are particularly unfavorable for demixing. These findings are consistent with the LLPS propensity predicted for regions of tau (30).

In the presence of 20 ng/μL RNA but the absence of PEG, 0N4R tau did not form droplets within 2 h (Fig. 1*D*), nor did most of the domain fragments. Importantly, the MTBD underwent LLPS in the presence of 20 ng/μL RNA alone (but no PEG) (Fig. 1 *E* and *F*, $P < 0.0001$, MTBD vs. 0N4R for % FOV and number of particles). These data suggested that some domains of 0N4R tau could inhibit the coacervation of MTBD occurring in the presence of RNA, possibly by competing for intra- or intermolecular interactions of 0N4R tau molecules. The MTBD and the proline-rich domains have a positive net charge (at pH 7.4), through which tau can establish nonspecific electrostatic interactions with RNA (5). The interaction of tau with RNA promotes fibrillization (similar to other polyanionic compounds such as heparin) (4) and inhibits tau-facilitated assembly of tubulin (5, 33). Our data indicate that the interaction of the positively charged proline-rich and microtubule binding domains with RNA seem to be particularly important for the physiological coacervation of tau. The interaction of RNA with the MTBD can thus facilitate both the phase separation and fibrillization of tau (4, 20).

We proceeded to explore whether phase separation of tau was sensitive to RNA sequence. Phase separation of tau is particularly efficient upon interaction with tRNA (20). tiRNAs are fragments of tRNA that are derived upon stress-induced angiogenin cleavage and are known to promote stress granule assembly (34–37). The small size of tiRNA provides a good system for exploring whether RNA sequence or secondary structure might affect tau phase separation. We used a library of tiRNAs to investigate whether tiRNAs (10 μM) differed in their ability to induce phase separation of 0N4R wild-type tau (5 μM) in the presence of 2% PEG. The resulting experiments showed differing efficiencies of tiRNAs in inducing tau phase separation (*SI Appendix*, Fig. S1 *D* and *E*), suggesting a role for RNA sequence or structure in promoting tau phase separation. 5′Ser, 5′Sec, and 5′Thr all induced more tau phase separation than total RNA ($^{**}P < 0.01$, ANOVA with Dunnett's post hoc comparison against RNA-induced control), while other tiRNAs (such as 5′Gln, 5′Lys, and 5′Asn, $^{***}P < 0.001$) failed to induce tau droplets. Minimum free energy (ΔG) structural analyses using the mfold algorithm (38) showed that the tiRNAs 5′Ser, 5′Sec, and 5′Thr share in common the presence of RNA stems that are eight or more bases in length, while all of the other tiRNAs tested

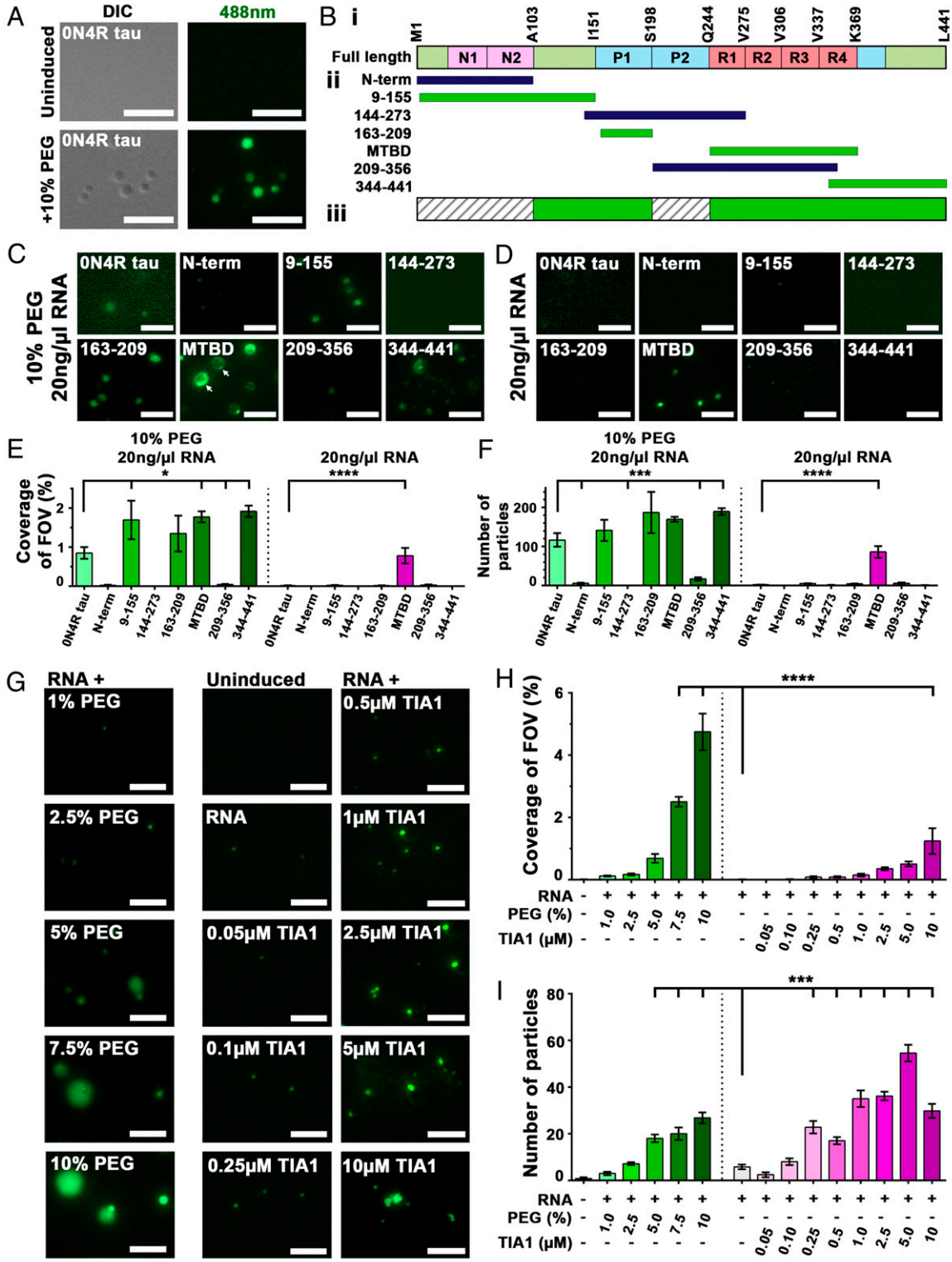

Fig. 1. RBPs substitute for crowding agent, allowing for phase separation of tau. (*A*) Phase separation of 0N4R tau-DL488 occurs in 10% PEG, leading to liquid droplets observable by DIC and fluorescent (λ488 nm) microscopy. (*B*, *i*) Schematic representation of 0N4R tau domains. (*B*, *ii*) Recombinant domains used for LLPS. Green domains undergo LLPS, blue indicates those that do not. (*B*, *iii*) Consensus mask of tau domains that favor LLPS (in green). (*C*) Phase separation of DyLight-488-conjugated tau domains in the presence of 10% PEG and 20 ng/µL RNA. (*D*) Quantification of 10% PEG and 20 ng/µL RNA induced tau-domain-488 droplets (from *C*) as coverage of field of view. (*E*) Phase separation of DL-488 conjugated tau domains in the presence of 20 ng/µL RNA (but no crowding agent). (*F*) Quantification of 20 ng/µL RNA induced tau-domain-488 droplets (from *E*) as coverage of field of view. (*G*) PEG functions as a crowding agent to facilitate phase separation of tau and RBPs. RBPs, here TIA1, can substitute for PEG to facilitate LLPS of tau into small granules that resemble those seen in neurons. (*H*) Quantification of tau-488 droplet formation as coverage of field of view. (*I*) Quantification of tau-488 droplet formation as number of particles formed. (Scale bars for *A*, *C*, *E*, and *G*: 5 µm.) For *D*, *F*, *H*, and *I*: $*P < 0.05$, $***P < 0.001$, $****P < 0.0001$. $n = 5$/group, mean ± SEM, ANOVA with Dunnett's post hoc comparison against RNA-only group).

showed RNA loops with smaller stems (*SI Appendix*, Fig. S1*F*). No consistent differences in primary sequence were observed. These data suggest that the secondary structure of RNA contributes to induction of tau protein phase separation.

Tau Phase Separation Is Facilitated by TIA1. In vitro crowding agents, such as PEG, mimic the molecular crowding that occurs in cells (32), but an accurate physiological understanding of this phenomenon benefits from evaluation of the biomolecules that are normally present in cells, interact with the target proteins, and facilitate tau phase separation. We hypothesized that RNA binding proteins, which frequently undergo RNA-induced LLPS (39) and are implicated in neurodegenerative disease pathogenesis, facilitate tau phase separation in vivo. In a three-component system (e.g., tau, RBP, and RNA) additional molecular interaction may confer favorable energetic conditions for phase separation. To test this, we observed in vitro phase separation of tau-488 in the presence of increasing concentrations of recombinant human TIA1 and compared it to the induction of tau-488 phase separation with increasing concentrations of PEG (all reactions were performed in the presence of 20 ng/μL RNA). Cytoplasmic phase separation of TIA1 is central for nucleation of nonmembrane bound SGs (27, 40) and is also recruited to tau neurofibrillary tangles in AD (22).

As expected, we found that phase separation of tau-488 in the presence of RNA depended on the concentration of PEG (Fig. 1*G*). PEG, both 7.5% and 10%, induced a significant increase in tau-488 droplets measured as percent coverage of FOV, droplet number, and area droplets (Fig. 1 *H* and *I* and *SI Appendix*, Fig. S1*G*, $P < 0.0001$, ANOVA with Dunnett's post hoc comparison against RNA-only control).

Importantly, in a dose-dependent manner, TIA1 was able to enhance the phase separation of tau-488 incubated in the presence of 20 ng/μL RNA but in the absence of PEG (Fig. 1*G*). A 2:1 molar ratio of TIA1:tau-488 (10 μM:5 μM) produced a significant increase in tau-488 droplet % coverage of FOV (Fig. 1*H*, $P < 0.0001$, ANOVA with Dunnett's post hoc comparison against the RNA-only control). Tau-488 droplets induced with TIA1 were smaller but more numerous than those induced with PEG alone (Fig. 1*I* and *SI Appendix*, Fig. S1*G*). As such, measuring the number of particles revealed that a significant increase in tau-488 droplets occurred with as little as 0.25 μM TIA1 (a molar ratio of 1:20, 0.25 μM TIA1:5 μM tau-488) (Fig. 1*I*, $P < 0.001$, ANOVA with Dunnett's post hoc comparison against the RNA-only control). The highest TIA1 concentration (molar ratio of 2:1, 10 μM TIA1:5 μM tau-488) showed fewer but larger droplets than with the optimal phase separation conditions of 1:1 molar ratio of 5 μM TIA1:5 μM tau-488. These data indicate that TIA1 promotes tau phase separation, indicating a physiological means by which this may occur in cells.

TIA1 Facilitates Vitrification of Phase-Separated Tau. The ability of TIA1 to facilitate partitioning of tau raised the question of the physical state of tau in the context of RBP-regulated phase separation. Analysis of tau-488 fluidity by fluorescent recovery after photobleaching (FRAP) indicated that phase-separated droplets became progressively more viscous over time (*SI Appendix*, Fig. S2*A*). Photobleached tau-488 droplets formed in the presence of 10% PEG and 20 ng/μL RNA exhibited less fluorescent recovery when incubated for 60 min before FRAP imaging, than when incubated for 40 or 20 min, consistent with a prior study (19).

Interestingly, the addition of TIA1 to the phase-separation reaction accelerated the decrease in fluidity of tau-488 droplets induced with PEG and RNA. At an early time point (<10 min), addition of 0.5 μM TIA1 was sufficient to prevent full recovery of tau-488 fluorescence following photobleaching, with fluidity being reduced even further in the presence of 5 μM TIA1 (Fig. 2*A* and *SI Appendix*, Fig. S2*B*; $P < 0.0001$ between each group, nonlinear one-phase association analysis). Fluorescent recovery of photobleached droplets consisting of tau alone is likely predominantly governed by diffusion rates of tau-488 within a fluid matrix, with diffusion decreasing as the droplets undergo gelation with time (*SI Appendix*, Fig. S2*A*). Enhanced gelation, occurring upon the interaction of tau with TIA1, further retards diffusion of tau-488 leading to rapid plateauing of the FRAP signal for tau-488. Thus, these data show that higher concentrations of TIA1 accelerate the gelation of copartitioned droplets of tau and TIA1.

Tau Shows Distinct Copartitioning Behavior Depending on RBPs. The enhanced vitrification (gelation) of tau droplets in the presence of TIA1 suggested copartitioning of tau and TIA1 in the liquid droplets that form, which could favor increased tau–tau intermolecular interactions. To test this hypothesis, we observed droplets formed by tau-488 incubated in the presence of PEG, RNA, and TIA1-594.

After 2 h, droplets composed of either 5 μM tau-488 or 5 μM TIA1-594 showed diffuse distribution of the proteins. However, in the presence of TIA1-594, tau-488 concentrated into small microdomains within larger TIA1-594 droplets (Fig. 2*B*). The distribution of tau-488 within TIA1-594 droplets became increasingly consolidated as the concentration of TIA1 increased, consistent with the tendency toward vitrification described above. At low concentrations of TIA1 (<0.5 μM TIA1, 10:1 ratio of tau:TIA1) most of the tau-488 and TIA1-594 remained diffuse in the droplets. At TIA1 concentrations >1.0 μM TIA1 (5:1 ratio of tau:TIA1), >50% of the tau concentrated into microdomains, while TIA1 at a concentration of 10 μM (1:2 ratio of tau:TIA1) leads to all tau being recruited into microdomains and substantial formation of microdomains of TIA1 (Fig. 2*C*). Observation of droplets by superresolution microscopy confirmed that at low concentration of TIA1 (0.5 μM), both tau-488 and TIA1-594 are diffuse within droplets, while tau-488 appears to already be concentrated within a TIA1-594 shell (*SI Appendix*, Fig. S2 *C* and *D*). At 5 μM TIA1, tau-488 microdomains were readily observable by superresolution microscopy and showed exclusion of TIA1-594 (Fig. 2*B* white arrows, *SI Appendix*, Fig. S2 *C* and *D*). This pattern of tau distribution within TIA1 is similar to interdroplet partitioning observed for the nucleolar proteins NPM1 and FIB1 based on differential droplet surface tension (41). Interestingly, phase separation of MTBD-488 with TIA1-594 (5 μM each) in the presence of PEG + RNA induced droplets that did not result in formation of microdomains (*SI Appendix*, Fig. S2*E*). This finding suggests that while interaction of MTBD, TIA1, and RNA can lead to copartitioning, other domains of tau are required for its further concentration into microdomains.

Tau exhibits a particular propensity to coaggregate with TIA1 in Alzheimer's brains (22), but also interacts with other RBPs in the disease state (25, 26). In order to explore how phase separation of tau was influenced by particular RBPs, we examined the interaction of tau with other RBPs (G3BP1, HNRNPA1, DDX6, RPL1, EIF4A1, and EIF4E) (*SI Appendix*, Fig. S3*E*). Surprisingly, in the absence of PEG but the presence of 20 ng/μL RNA, tau phase separation induced by G3BP1 was only ∼10% of that induced by TIA1, with small tau-488 droplets becoming apparent only at 2.5 to 5 μM G3BP1 (*SI Appendix*, Fig. S3 *A–D*) compared to 0.05 to 0.1 μM of TIA1 (Fig. 1 *G–I*). None of the other RBPs tested induced significant phase separation of tau-488. These data suggested that TIA1 exhibits a selective capability to promote tau phase separation.

To better understand the interaction of tau within RBP droplets, we studied tau-488 distribution upon demixing in the presence of PEG and recombinant RBPs. Tau-488 (5 μM) was mixed with 10% PEG, 20 ng/μL RNA, and different RBPs labeled with DyLight-594 at concentrations ranging from 0 to

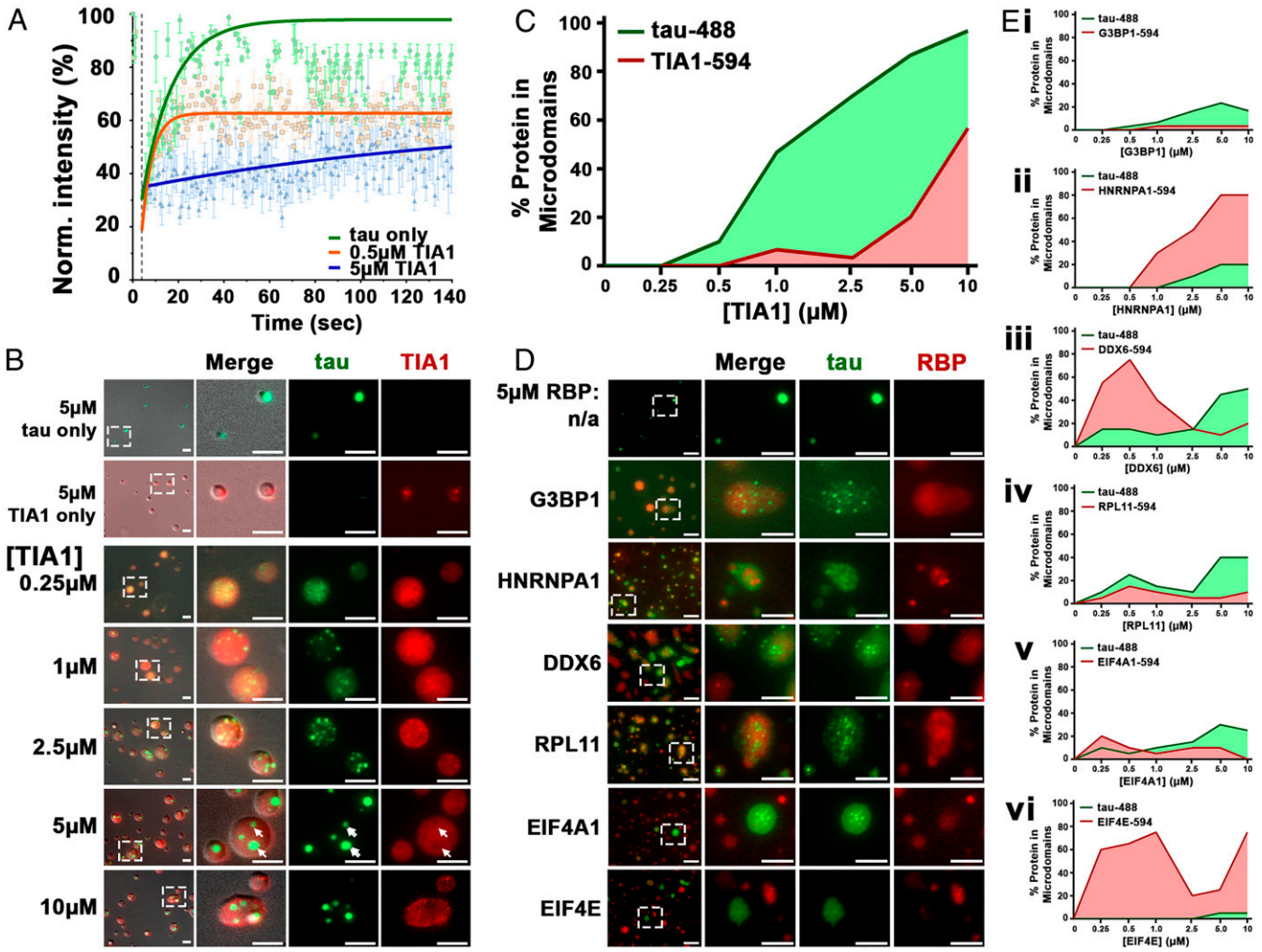

Fig. 2. TIA1 facilitates gelation of phase-separated tau. (*A*) When cophase separating with TIA1, 5 μM tau-488 shows gelation in a dose-dependent manner. Timed fluorescent recovery after photobleaching of phase-separated tau-488 droplets (*SI Appendix*, Fig. S2*B*) was assessed immediately after induction with 10% PEG and 20 ng/μL RNA in the presence or absence of TIA1. (*B*) In a dose-dependent manner, increasing TIA1-594 causes concentration and redistribution of tau-488 into microdomains within TIA1-594 droplets. At high TIA1-594 concentration, tau microdomains show asymmetric distribution (arrowheads). Tau-488 microdomains exclude TIA1-594 (arrows, also see *SI Appendix*, Fig. S2 *C* and *D*). (*C*) Quantification of percent of tau-488 and TIA-594 protein in concentrated microdomains. (*D*) The properties of tau-488 phase separation are affected by various RBPs (images shown for 5 μM tau-488 and 5 μM RBP-594). (*E*) Quantification of RBP-594 concentration-dependent microdomain formation of tau-488 (5 μM) and of (*E*, *i*) G3BP1-594; (*E*, *ii*) HNRNPA1-594; (*E*, *iii*) DDX6-594; (*E*, *iv*) RPL11-594; (*E*, *v*) EIF4A1-594; and (*E*, *vi*) EIF4E-594. (Scale bars: 5 μm.)

10 μM (Fig. 2 *D* and *E*). The resulting protein condensates showed three different partitioning behaviors (*SI Appendix*, Table S1 and Fig. 2 *D* and *E*): 1) tau forms microdomains inside of RBP droplets "(tau|RBP)," where the RBP is TIA1, G3BP1, DDX6, or RPL11; 2) RBP forms microdomains inside tau droplets "(RBP|tau)," where the RBP is HNRNPHA1; and 3) tau or RBP droplets form independently "(tau)(RBP)," where the RBP is EIF4E. Furthermore, the pattern of partitioning of tau with other RBPs was dependent upon RBP concentration. For example, DDX6 at low concentration (~0.5 μM) forms microdomains within tau-488 (5 μM) droplets, but at higher concentration (>2.5 μM) recruits tau-488 into microdomains (Fig. 2 *E*, *iii*). This indicates that tau copartitioning with RBPs is regulated by the molecular ratio of tau:RBPs, similar to what has been observed for the molecular ratio of RBPs:RNA in FUS LLPS (42).

The pattern of partitioning was also pH dependent. The isoelectric points (pIs) of tau and EIF4A1 are 10.1 and 5.1, respectively (*SI Appendix*, Fig. S3*F*). At pH ≤ 5, EIF4A1 becomes positively charged (as is tau), and tau formed condensed globules that contained only a little EIF4A1 (*SI Appendix*, Fig. S3*G*). At pH ≥ 6, tau-488 and EIF4A1-594 copartitioned into droplets that exhibit two types of behavior, copartitioning or independent partitioning. The variable nature of particles at pH > 6 may be due in part to changes in protein net charge (and single amino acid residue charges) that occur in tau and EIF4A1 in this pH range, which change the electrostatic interactions between tau and tau, tau and EIF4A1, and EIF4A1 and EIF4A1. The "balance of charges" has previously been shown to be important for the coacervation of tau with RNA (20). The compositional variations of tau:RBP condensates also suggests a role for stochastic factors, such as the balance of charges in small condensates, in determining the nature of the protein droplet as the tau or EIF4A1 protein begin to phase separate. Thus, the electrostatic properties of RBPs and tau contribute to their patterns of partitioning in a process that might also have stochastic behavior.

In principle, the loss of entropy during liquid–liquid phase separation of a protein is unfavorable. This energy cost must be balanced by the enthalpic gain generated by homogenous and heterogeneous molecular interactions in the system. For a

cophase separation system, e.g., (tau|RBP) and (RBP|tau), heterogeneous interactions between protein species A (i.e., tau) and species B (i.e., RBPs) enable copartitioning into the same droplet, resulting in a negative change in free energy (*SI Appendix*, Table S1, summed tensor field $\Sigma\nabla\varepsilon < 0$). This is not the case for proteins that form independent phase-separating droplets, such as occurs with tau and EIF4E (Fig. 2*D*). In circumstances where microdomains occur, the species that forms microdomains exhibits stronger homogenous interactions, with interactions that are sufficiently strong leading to exclusion of the other species (*SI Appendix*, Table S1). As an example, in the presence of TIA1, the homogenous interactions of tau–tau exhibit a greater enthalpy than the sum of homogenous TIA1–TIA1 interactions and the heterogeneous interactions of tau with TIA1, leading to formation of tau microdomains within TIA1 droplets.

RNA and TIA1 Facilitate Oligomerization of Tau. Understanding the relative toxicities of semisoluble oligomers and insoluble fibrils is one of the most important biochemical questions in the field of tau-related neurodegenerative research. The accumulation of NFTs, composed of f.tau, correlates with cognitive decline in AD. However, studies of animal models suggests that, rather than NFTs, o.tau is the neurotoxic species (11, 43–48). Recent studies demonstrate that reduced o.tau and increased f.tau correlated with improved behavioral performance and survival in PS19 tau transgenic mice (8). This occurred in response to depletion of endogenous TIA1, indicating that TIA1 is responsible for the accumulation of o.tau. In order to understand how tau phase separation relates to each of these states, we compared the effects of TIA1, RNA, and PEG on the accumulation of o.tau and f.tau, and stages of tau LLPS, including l.tau and v.tau. We used stained NativePAGE, thioflavin S (ThS) fibrillization assays, dot blots, and enzyme-linked immunosorbent assays (ELISAs) to identify each species (Fig. 3).

Phase separation of tau (l.tau) in the presence of 10% PEG (+ RNA) did not produce tau oligomers or high molecular weight material, as observed by NativePAGE stained with Coomassie blue or silver stain (Fig. 3 *A* and *B* and *SI Appendix*, Fig. S4*A*). PEG (+ RNA) also reduced the formation of ThS-positive tau fibrils compared to RNA alone (Fig. 3*C* and *SI Appendix*, Fig. S4*C*) and no fibrils were detected in reactions of tau + PEG + RNA by transmission electron microscopy (TEM) (*SI Appendix*, Fig. S4*D*). Interestingly, the vitrification of tau droplets (v.tau) induced in the presence of TIA1, PEG, and RNA similarly produced neither tau oligomers nor ThS-positive fibrils. The absence of oligomeric tau in tau droplets formed in the presence of PEG + RNA (± TIA1) was confirmed by ELISA (Fig. 3 *D*, *iii* and *iv* and *SI Appendix*, Fig. S5*A*) and dot blot (Fig. 3 *E* and *F* and *SI Appendix*, Fig. S5 *B–G*) using antibodies specific for oligomeric tau (TOC1).

Although the incubation of tau with 20 ng/μL RNA (but no PEG) induced little phase separation (Fig. 1), it immediately (t = 0 h) led to accumulation of tau oligomers that are observed by NativePAGE as distinct bands of increasing molecular weight (~80 kDa) (Fig. 3*A*, lanes 5). The o.tau generated by the addition of RNA continued to accumulate over time (Fig. 3*A* and *SI Appendix*, Fig. S4*A*). High molecular weight f.tau also accumulated over time in the presence of RNA, as identified by ThS assay (Fig. 3*C* and *SI Appendix*, Fig. S4*B*) and silver stain (Fig. 3*B*). However, the rate of f.tau accumulation was much slower than the rate for o.tau production, consistent with prior reports suggesting that production of o.tau occurs as an intermediate stage of RNA-induced tau fibrillization (8, 12). The presence of RNA led to production of tau fibrils that were detected by TEM (*SI Appendix*, Fig. S4*D*); these fibrils were found to be similar to those induced by another polyanionic compound, dextran sulfate.

Notably, the addition of TIA1 increased the accumulation of o.tau in reactions containing 20 ng/μL RNA but no PEG (Fig. 3*D*). ELISAs using o.tau-specific antibody TOC1 (49) and misfolded tau antibody TNT1 (recognizing exposure of the phosphatase-activating domain [PAD]) (50), showed that addition of 5 μM TIA1 to reactions of 5 μM tau and 20 ng/μL RNA produced a significant increase in TOC1 (Fig. 3 *D*, *i*) and TNT1 (*SI Appendix*, Fig. S3 *D*, *iii*) reactivity compared to uninduced tau ($P < 0.0001$, ANOVA with Tukey's post hoc comparison). Furthermore, o.tau produced in the presence of TIA1 (+ RNA) resulted in significantly more TOC1 reactivity by ELISA than tau incubated with RNA alone ($P < 0.001$). These findings were confirmed by dot blot and immunolabeling with TOC1 antibody (Fig. 3*E* and *SI Appendix*, Fig. S5 *B–G*). Quantification of dot blot signal showed that addition of TIA1 and RNA to tau (5 μM each protein) increased the formation of TOC1-positive o.tau (Fig. 3*F*; compared to uninduced tau or tau with RNA alone; $P < 0.001$, ANOVA with Tukey's post hoc comparison). Accumulation of TOC1-positive o.tau occurred rapidly in reactions containing tau + TIA1 + RNA (without PEG) (<5 min; *SI Appendix*, Fig. S5*D*) and with as little as 1 μM TIA1 (*SI Appendix*, Fig. S5 *B* and *C*). NativePAGE analysis suggests that the presence of TIA1 inhibited the accumulation of tau multimers more than ~150 kDa identified by Coomassie staining (Fig. 3*A*), although silver stain did show some high molecular weight material (Fig. 3*B*). TIA1 also inhibited the accumulation of ThS-positive TEM detectable fibrils in reactions containing 20 ng/μL RNA (Fig. 3*C* and *SI Appendix*, Fig. S4*D*), similar to our previous findings using solutions containing tau and dextran sulfate (8).

Because TIA1 colocalizes with tau pathology in AD brains (22) and can drive phase separation of tau (Fig. 1 *G–I*) in a manner that G3BP1 does not (*SI Appendix*, Fig. S3 *A–D*), we explored whether TIA1 has a selective ability to facilitate oligomerization of tau. While addition of RNA and TIA1 to tau led to accumulation of TOC1-positive o.tau over a 4-h period, addition of RNA and G3BP1 or other RBPs (HNRNPA1 and EIF4E) did not result in accumulation of o.tau compared to tau incubated with RNA alone (Fig. 3*G* and *SI Appendix*, Fig. S6*A*). Interaction of tau with TIA1 likely requires RNA as an intermediate (25). Hence, we investigated the role played by the RNA recognition motifs (RRMs) of TIA1 in development of o.tau. Incubation of tau with RNA and GST-tagged TIA1 (5 μM; both long NP_071505.2, and short NP_071320.2 isoforms) reproduced the critical finding that TIA1 facilitates generation of o.tau (Fig. 3*H* and *SI Appendix*, Fig. S6*B*). GST-fusion proteins containing individual TIA1 RRMs (RRM1, RRM2, and RRM3) or RRMS in pairs (RRM1/2 and RRM2/3) did not generate significantly more TOC1 immunoreactivity compared to tau incubated with GST alone. This finding suggests that the interaction of TIA1 RRMs with RNA and tau which leads to the production of o.tau may depend in part on the presence of the IDR. To fully explore this idea, we substituted the IDR of TIA1 with orthologous G3BP1 "RGG" or HNRNPA1 IDR domains (*SI Appendix*, Fig. S6 *C* and *D*). These domains are necessary for the phase separation into stress granules of each respective RBP (27, 51–53). TIA1 hybrids, in which the endogenous IDR (glycine-rich domain) was substituted with that of G3BP1 or HNRNPA1, did not drive formation of o.tau in the presence of RNA (Fig. 3*I* and *SI Appendix*, Fig. S6*E*), confirming that the TIA1 IDR is necessary for facilitating production of o.tau. In summary, we found that TIA1 selectively promotes the formation of smaller (<150 kDa) o.tau species while inhibiting the formation of RNA-induced f.tau, perhaps reflecting a delayed conversion of oligomers into high molecular weight fibrils.

Oligomeric Tau Causes Toxicity and Neurodegeneration. Next, we evaluated the neurotoxicity of each tau species produced by RNA-induced tau phase separation in the presence or absence of

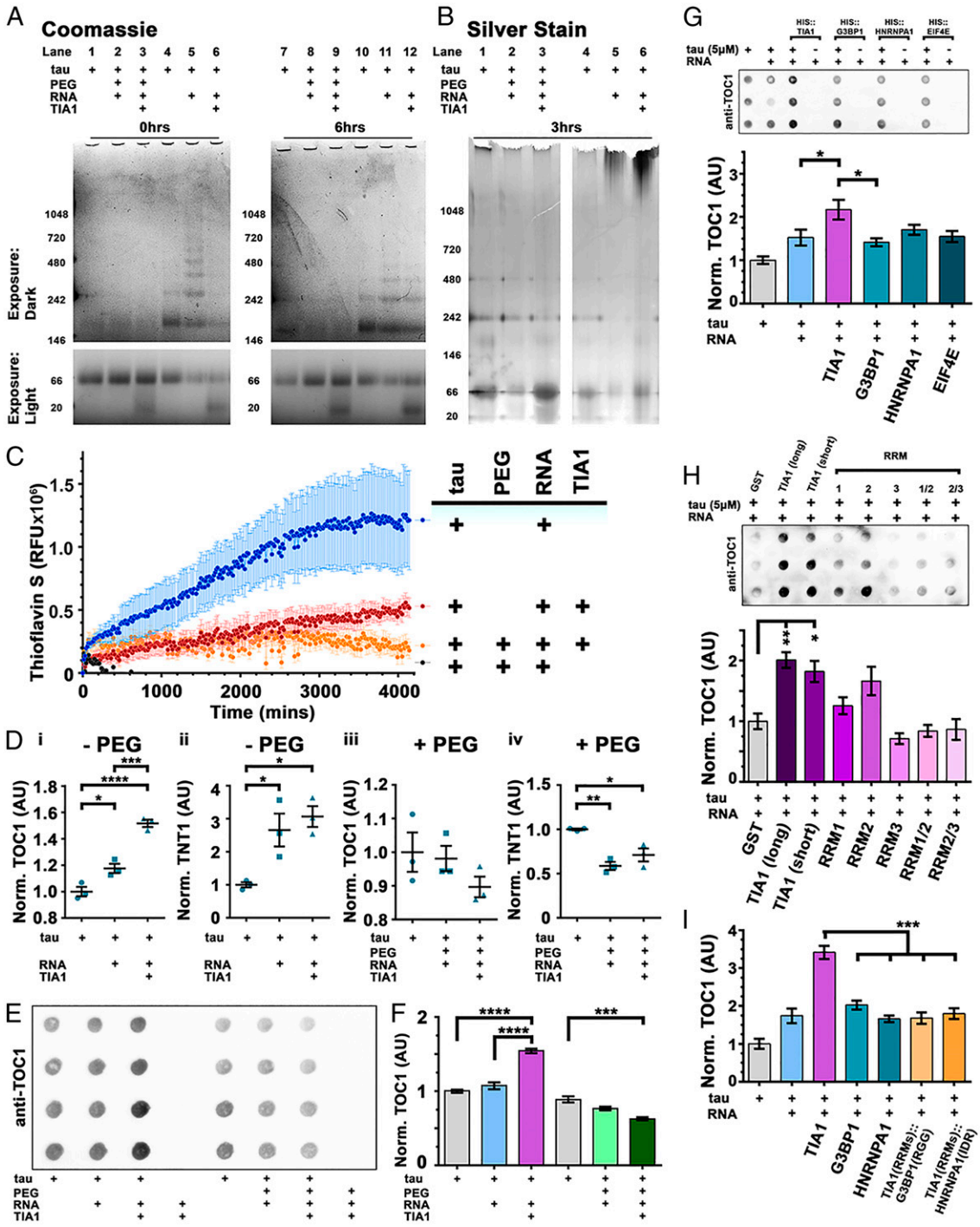

Fig. 3. RNA and TIA1 (but not PEG) facilitates oligomerization of tau. (*A*) NativePAGE with Coomassie shows little multimerization in tau upon addition of PEG-8000, even upon addition of TIA1. Tau induced with RNA rapidly forms many sized multimers in a time-dependent manner, but the size is limited by addition of TIA1. (*B*) Silver stain shows little high molecular weight material forms upon PEG induction. RNA-only induction of tau multimers, ± TIA1, shows accumulation of high molecular weight material. (*C*) Thioflavin S fluorescent assay shows time-dependent formation of amyloid fibrils in tau samples that are polymerized with RNA alone. (RFU, relative fluorescent units. n = 4/group, mean ± SEM). (*D*) ELISAs detecting oligomeric tau (TOC1 antibody) or conformationally altered tau (TNT1 antibody), indicate that RNA triggers significant accumulation of both TOC1 (*D*, *i*) and TNT1 (*D*, *ii*) immunoreactive tau. However, in the presence of TIA1 (+RNA), tau forms significantly more TOC1-positive oligomeric tau than RNA induction alone (*D*, *i*). (n = 3/group, mean ± SEM). PEG induction, ± TIA1, leads to no formation of tau oligomers (*D*, *iii*) and a significant reduction in TNT1 conformationally changed tau (*D*, *iv*). (n = 3/group, mean ± SEM). (*E*) Oligomerization of tau observed by dot blots immunolabeled with anti-oligomeric tau antibody TOC1. (*F*) Quantification of dot densitometry (from *E*) shows that tau undergoes significant oligomerization in the presence of RNA (20 ng/μL) and TIA1 (5 μM). PEG + TIA1-induced tau has significantly less TOC1 reactivity than uninduced control. (n = 4/group, mean ± SEM). (*G*) Oligomerization of tau is selectively facilitated by the RBP TIA1. (*H*) GST-tagged TIA1 facilitates oligomerization of tau. Recombinant proteins lacking the IDR generate less o.tau. (*I*) Hybrid RBPs consisting of the RRMs of TIA1 and the IDR of either G3BP1 or HNRNPA1 do not facilitate oligomerization of tau. (n = 6/group, mean ± SEM). (AU, arbitrary units. *P < 0.05, **P < 0.01, ***P < 0.001, ****P < 0.0001. ANOVA with Tukey's post hoc comparison between all groups).

PEG or TIA1. We previously described how o.tau seeding modulates the translational stress response of human tau expressing primary hippocampal neurons, while f.tau seeds inclusions that recruit p62/SQSTM1 and are targeted to the autolysomal cascade (54). Tau seeds spread between cells via the LRP1 receptor (55), resulting in conversion of endogenous tau into the conformation of the seeded material (56).

We chose five conditions, each of which produces a mixture containing one predominant conformation of tau: 1) f.tau = tau + RNA (incubated for 24 h), 2) o.tau = tau + TIA1 + RNA (incubated for 6 h), 3) l.tau = tau + PEG + RNA (incubated for 2 h), 4) v.tau = tau + TIA1 + PEG + RNA (incubated for 2 h), and 5) monomeric tau (m.tau). Cultured primary hippocampal mouse neurons were treated with the different tau preparations (total tau concentrations ranging from 0.16 μg/mL to 20 μg/mL) for 7 d (from days in vitro [DIV]7 to DIV14). Upon completion of treatment, the culture media were collected and assayed for lactate dehydrogenase (LDH) release indicative of cell death, then the cells were fixed, and MAP2 immunopositive cells were counted to quantify cell viability. As a positive control of toxic tau exposure, primary neurons were treated with a semisoluble biochemical fractionation (S1p) collected from PS19 transgenic tau mouse brain that was previously shown to be enriched for o.tau (described in ref. 9). S1p is the pelleted material obtained from the second high-speed centrifugation of TBS-extractable brain supernatant (8).

As expected, treatment of the neurons with S1p caused significant loss of MAP2-positive neurons (Fig. 4 *A* and *C*, $^{**}P < 0.01$, ANOVA with Tukey's post hoc comparison); however, LDH release was similar to control-treated neurons. In contrast, addition of o.tau caused a dose-dependent increase in LDH release and loss of neurons (*SI Appendix*, Fig. S7 *A–C*). At the highest dose of 20 μg/mL o.tau, a significant change in LDH release and MAP2-positve neurons was observed compared to vehicle-treated controls (Fig. 4 *A–C*, $^{**}P < 0.01$, $^{***}P < 0.001$, ANOVA with Tukey's post hoc comparison).

Interestingly, addition of f.tau to primary neurons appeared to increase LDH release and decrease MAP2-positive neurons in a dose-dependent manner (*SI Appendix*, Fig. S7 *A–C*), but these changes were weaker than from exposure to o.tau. LDH release and MAP2-positive neuron counts in the presence of f.tau treatment (even at the highest concentration) did not show statistically significant differences when compared to treatment with vehicle alone (ANOVA with Tukey's post hoc comparison of all groups). Residual TOC1-positive tau oligomers are present in f.tau samples (generated by incubating tau with RNA; Fig. 3 *D*, *i*), because oligomers are necessary intermediaries in the production of fibrils. Such residual o.tau could therefore be responsible for the partial toxicity associated with f.tau treatment. We also observed that addition of l.tau or v.tau induced no toxicity in cultured primary neurons, even at the highest concentration of 20 μg/mL tau. To exclude the impact of TIA1 itself on cell viability in this assay, the concentration of TIA1 was kept constant in all experiments by supplementing the culture medium with monomeric TIA1 for f.tau or l.tau treatments. Combining the multiple lines of evidence in the current study with the strong evidence of the specific toxicity of TIA1-dependent o.tau in transgenic mice (8, 9, 46–49, 57–59) indicates that the presence of TIA1 in tau droplets produces o.tau species with especially high neurotoxic potential.

Discussion

In this manuscript, we show that the interaction of tau with RNA and the RNA binding protein TIA1 is sufficient to drive phase separation of tau at physiological protein concentrations, without requirement of artificial crowding agents such as PEG. Using this system, we demonstrate that TIA1 also promotes tau oligomerization and vitrification. Interestingly, we find that TIA1 exhibits a selective ability to copartition with tau under physiological conditions, which speaks to the importance of TIA1 in tau biology. Other RBPs, such as G3BP1, are able to copartition with tau, but this happens only in the presence of crowding agents. Finally, we observe that the o.tau produced by in vitro interactions with TIA1 and RNA is highly neurotoxic, unlike other conformers of tau produced in vitro.

Fig. 4*D* presents a potential model describing the relationship between different (patho)physiological tau states. RNA induces the oligomerization (i) and subsequent fibrillization (ii) of tau. The presence of TIA1 (iii) shifts the reaction diagram to favor the accumulation of o.tau over f.tau, leading to an increased abundance of toxic o.tau (iv). The presence of TIA1 increases neurotoxicity (8), since o.tau is more toxic than f.tau (v). In the presence of PEG, l.tau is formed by demixing from the aqueous phase (vi); a process, which in vivo, may be a means to nucleate microtubule assembly (16). Over time (vii), liquid droplets of tau gelate into v.tau (viii) (19); this process could be accelerated by oligomers, which are more abundant in the presence of TIA1.

The work presented herein investigates two critical related biochemical processes, the processes generating phase separated tau and neurotoxic tau. LLPS is a fundamental biological process that derives from core biophysical principles revolving around free energy and entropy. In the cell, LLPS is used for the formation of membraneless organelles (14, 15). Recent work indicates that phase separation is modulated by both weak interactions, such as those associated with Pi–cation interactions, and higher affinity interactions, which can result from high affinity binding sites producing a multivalent system (28, 29). Cellular membraneless organelles, such as SGs or P-bodies, are diverse and complex mixtures of different proteins and RNA that function in concert (60). Tau selectively associates with stress granules that contain the RBP TIA1 (22, 23), and both tau and TIA1 can phase separate in vitro (19, 20, 61, 62).

Here we use the interaction of tau with RBPs to investigate whether the biophysical properties of these proteins are sufficient to drive copartitioning of tau with RBPs and to elucidate the specific phase behavior of these heterogeneous mixtures. We found that tau undergoes phase separation at or approaching physiological concentrations (1 to 5 μM) (63–66) when the process occurs in the presence of TIA1 and RNA (notably, in the absence of molecular crowding agents). The interaction between tau and TIA1 appears to be selective because other RBPs that we tested did not drive tau phase separation under physiological conditions without artificial crowding. Interestingly, although G3BP is a classic SG nucleating protein, tau does not phase separate with G3BP1 granules in cells (22), nor with recombinant G3BP1 in absence of crowding agents. Thus, these copartitioning studies demonstrate that tau is highly sensitive to the biophysical properties of TIA1. Such molecular specificity suggests that biophysical properties favoring the copartitioning of functionally linked proteins could be a fundamental process leading to the diverse array of cellular membraneless organelles.

In neurodegenerative tauopathies, the physical state of tau is linked to its neurotoxic potential. Whereas soluble monomeric/dimeric tau is important for the regulation of microtubule stability (and other less-known cellular processes), small oligomeric tau species appear to be highly neuro- and synaptotoxic (46–49, 57–59), and larger fibrillar tau aggregates do not appear to be very toxic (43, 44). For instance, in vivo propagation studies show that both soluble tau oligomers and insoluble tau fibrils spread tau pathology upon intracranial injection in mice (9, 11). However, only injection of tau oligomers causes neurotoxicity in the murine brain (9, 10), while treatment of cells with recombinant tau fibrils (that are then sonicated) propagates aggregates without inducing cell death (67). In vitro studies show that recombinant tau readily forms fibrils in the presence of polyanionic agents, such as RNA, but the resulting aggregated tau

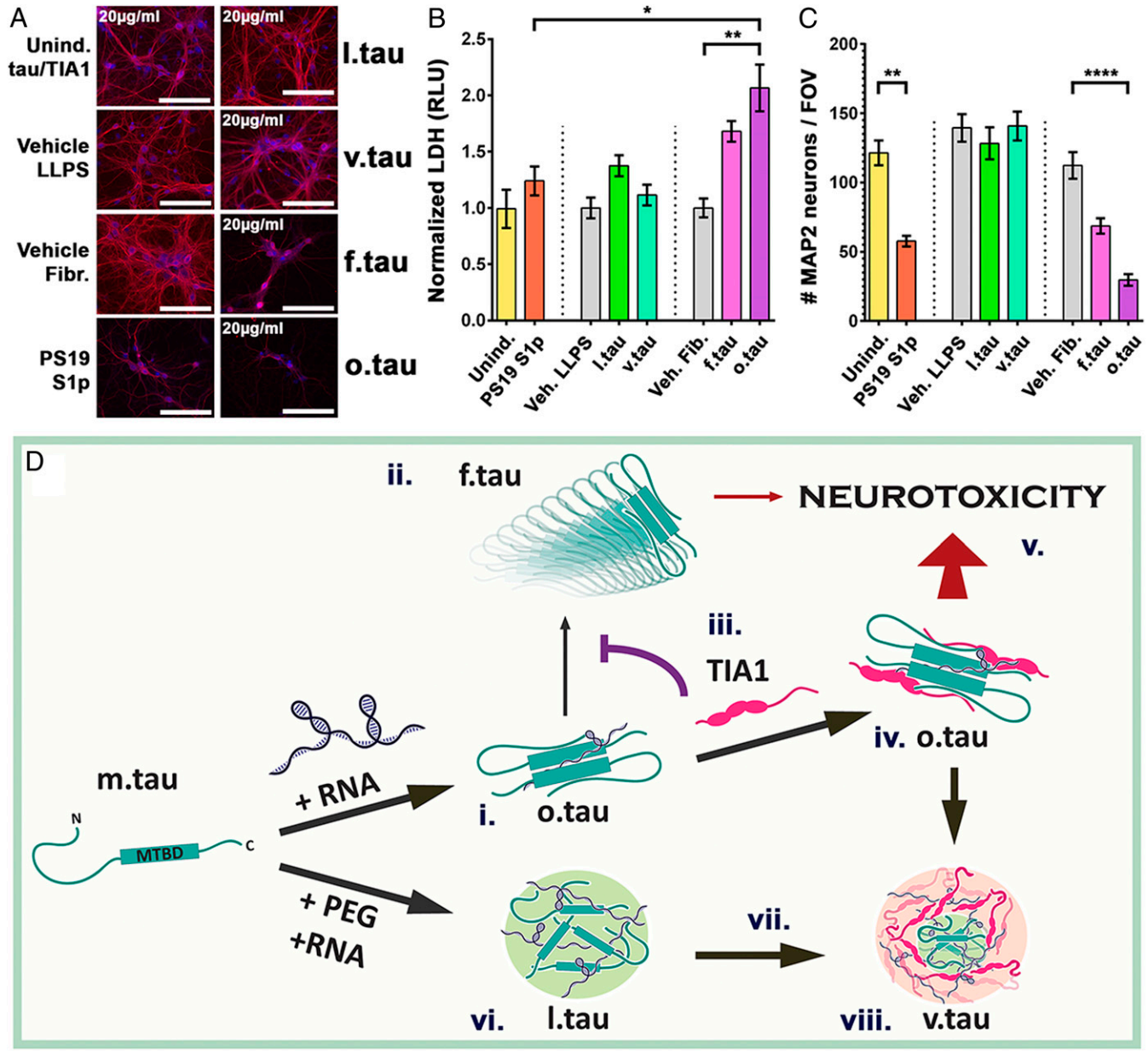

Fig. 4. RNA- and TIA1-induced oligomeric tau is neurotoxic. (*A*) Primary hippocampal neurons were assayed for toxicity and viability following treatment for 7 d with l.tau, v.tau, f.tau, and o.tau. Neurons are labeled with MAP2 (red) and counterstained with DAPI (blue). Negative controls: uninduced tau and TIA1; vehicles for LLPS and fibrillization reactions. Positive control: S1p biochemical fraction from PS19 mice. (Scale bar: 100 µm.) (*B*) Quantification of LDH release from primary neurons shows that o.tau treatment causes toxicity (RLU, relative luminescent units). (*C*) Quantification of MAP2-positive neuron count shows that o.tau treatment causes neuronal death. (For *B* and *C*: n = 3/group, mean ± SEM $^{*}P < 0.05$, $^{**}P < 0.01$, $^{****}P < 0.0001$. ANOVA with Tukey's post hoc comparison between all groups). (*D*) Schematic diagram of progression of tau from m.tau into higher order species. TIA1 prevents conversion of o.tau into f.tau (iii) leading to increased o.tau abundance which drives neurotoxicity.

species are not particularly toxic (4). Recent work also showed that prolonged LLPS of tau leads to the adoption of known pathogenic conformations of tau such as oligomers and N-terminal exposure, but this was following incubation with PEG and neurotoxicity was not assessed (24). The weak toxicity of tau fibrils and tau complexes generated in vitro suggests a critical hole in our understanding of the generation of toxic tau conformation.

The work presented in this manuscript bridges this fundamental gap in our understanding of tau biology by showing that tau exhibits a striking transformation when copartitioning with TIA1 and RNA. Tau rapidly forms oligomers when mixed with RNA alone, then shows progressive conversion into fibrils with time. In the presence of TIA1, tau initially appears homogenously dispersed within TIA1 droplets, suggesting comiscibility. Tau then consolidates into microdomains that exclude TIA1, and the tau becomes progressively gelated; these tau microdomains could be hubs for the formation of oligiomeric tau species. TIA1 inhibits conversion of tau oligomers to tau fibrils, which promotes the accumulation of tau oligomerization and is associated with accelerated tau vitrification. Recent work showing liquid RBP phases are nucleated by preformed oligomers (68) supports a hypothesis that the interaction of tau with TIA1 in SGs could accelerate tau LLPS, vitrification, and formation of toxic

oligomers. These observations suggest an important role for TIA1 in the accumulation of tau oligomers in the pathophysiology of AD (8).

In summary, we now provide a comprehensive model that describes the relationship between tau oligomerization, fibrillization, phase separation, and neurotoxicity. These studies also generalize to provide profound insight into mechanisms governing formation of physiologically selective membraneless organelles containing specific proteins, and thereby explain how cellular LLPS can impose specific functional attributes to different RNA granules.

Materials and Methods

Recombinant Proteins and RNA Preparation. 0N4R tau was made as previously described (69). Briefly, human 0N4R wild-type (WT) tau was expressed in Rosetta DE3 (Novagen) bacteria using IPTG (isopropyl β-D-1-thiogalactopyranoside) from the pET30a vector, then extracted by freeze/thaw lysis, purified by HiTrap SP HP (GE) ion-exchange column, and dialyzed into 10 mM Hepes buffer at pH 7.4.

Recombinant human RBPs were cloned into the pET28a vector for in-frame fusion with an N-terminal 6×HIS tag, then sequenced and transformed into SoluBL21 competent cells (Genlantis). Briefly, recombinant RBPs were isolated by HiTrap chelating (GE) affinity purification then HiPrep 26/60 S-200 (GE) size exclusion chromatography (*SI Appendix, Materials and Methods*). Recombinant proteins were fluorescently labeled with DyLight-488 or DyLight-594 (as indicated) using the Abcam DyLight Fast Conjugation Kit. Reactive dye was dissolved in 10 mM Hepes pH 7.4 for a stock concentration of 1 mg/mL 1:10 vol/vol. DyLight modifier was added to 20 μg protein, before addition of ∼1 μg of appropriate DyLight conjugate. The solution was mixed and incubated in the dark for 15 min at room temperature (RT). The 1:10 vol/vol quencher was then added for an incubation period of 5 min at RT. For experimental reactions (to provide an optimal quantum yield), fluorescently labeled proteins were mixed 1:3 to 1:5 with unlabeled protein from the same purification preparation (i.e., 1 part TIA1-594 mixed with 4 parts TIA1).

Total murine brain RNA was collected from snap frozen whole hemispheres dissected from isofluorane-killed, phosphate-buffered saline (PBS)-perfused C57Bl6 mice. RNA was extracted by tissue lysis in QIAzol reagent following the Lipid Tissue RNeasy Minikit protocol (Qiagen).

Phase-Separation and Fibrillization Reactions. Unless otherwise indicated, phase-separation reactions were performed on 5 μM 0N4R WT tau in 10 mM Hepes pH 7.4, 100 mM NaCl, 10% PEG (PEG-8000), 20 ng/μL total murine brain RNA and 1.5% glycerol (which is carried into the reactions with the recombinant RBPs). Proteins were mixed in PCR tubes, induced, and then 3 μL was spotted to wells on microscope slides made by SecureSeal Imaging Spacers (SS10 × 6.35; Grace Bio-Laboratories), coverslipped, then inverted (allowing forming droplets to settle by gravity onto coverslips), and incubated at 24 °C for 2 h (or indicated time). Unless otherwise indicated, fibrillization reactions were performed 5 μM 0N4R WT tau in 10 mM Hepes pH 7.4, 100 mM NaCl, 1 mM dithiothreitol (DTT), and induced with 20 ng/μL total murine brain RNA. Proteins were mixed in PCR tubes, induced, and then incubated with agitation at 37 °C for 6 h (or indicated time).

Microscopy and Quantification of Droplets. Fluorescently labeled droplets in imaging spacers were routinely imaged at 63× on a Zeiss AxioObserver A1 epifluorescent microscope equipped with DIC. Quantification of size distribution and number of particles was performed using MatLab and ImageJ. Microdomains were scored by three blinded individuals as percent of diffuse proteins versus protein concentrated into microdomains (*SI Appendix, Materials and Methods*).

Fluorescent Recovery after Photobleaching. FRAP experiments were performed on droplets formed by 10% PEG and 20 ng/μL RNA induction of WT 0N4R DyLight-488 on a Zeiss LSM880 confocal microscope with a 40× objective. Time-dependent gelation was performed on tau-488 droplets formed after 20-min, 40-min, and 60-min incubations. TIA1 regulation of tau-488 droplet fluidity was tested at the ∼0-h time point with addition of 0 μM TIA1, 0.5 μM TIA1, or 5 μM TIA1. For 5 to 10 droplets per field of view in triplicate experimental reactions, subregions of 0.15 μm^2 were defined to follow change in intensity. In each experiment, two regions outside of droplets and two unbleached regions within droplets were imaged for normalization to background and for drift. Experimental regions were bleached at 100% transmission (∼35 mW for argon 488/∼2 mW for HeNE 594) for 1 to 2 min. Postbleach, time-lapse images were collected (1-s frame rate, 120 frames) and analyzed with MatLab. Mean fluorescence intensities of regions were recorded by time point then normalized as follows:

$$Intensity\ Time(x)_{Experimental\ region} = \left(\frac{Intensity\ Time(x)_{Experimental\ region} - Intensity\ Time(x)_{Background}}{Intensity\ Time(x)_{Unbleached\ region} - Intensity\ Time(x)_{Background}}\right)$$

Experimental region intensities by time point were then transformed as a percentage of the corresponding experimental region intensity prior to bleaching. Fluorescent intensities were plotted against time using GraphPad Prism. Statistical comparison of recovery rates between treatment groups was made by fitting nonlinear one-phase association curve equations.

Biochemical Analyses: Fibrillization, NativePAGE, Dot Blot, and ELISA. ThS (Sigma) solution was freshly prepared at a concentration of 500 μM in water. LLPS and fibrillization reactions (5 μL of 10 μM tau in quadruplicate) were incubated in 384 well plates in the presence of 20 μM ThS and read every 15 min at 440 nm/485 nm in a SpectraMax i3× plate reader. Signal was normalized by subtraction of vehicle blank, then transformation against initial (time = 0) uninduced sample signal.

Samples of reacted tau (500 ng/lane) were resolved by NativePAGE 4–16% Bis-Tris gel (Thermo) according to manufacturer's protocol. Gels were washed (3 × 15 min) in deionized H_2O, then fixed by microwaving (45 s) in 40% methanol/10% acetic acid, then incubating overnight at RT in fixative. Gels were washed again (3 × 15 min) with water and stained with either Coomassie (SimplyBlue, Thermo) or silver stain (SilverQuest, Invitrogen). For dot blotting, a 0.45-μm nitrocellulose membrane was rinsed in buffer (10 mM Hepes pH 7.4, 50 mM NaCl), then placed on filter paper in a Bio-Dot Apparatus (Bio-Rad). Buffer (200 μL) was pulled through by vacuum three times, then tau samples (100 ng/well) were diluted in 100 μL buffer and applied to the dot blot by vacuum. Buffer (200 μL) was pulled through each well an additional three times. Membranes were blocked 1 h at RT in 5% milk in PBS, washed in PBS, then probed overnight with the following antibodies: (mouse) anti-oligomeric tau TOC1 (1:1,000); (mouse) anti-tau conformation TNT1 (1:1,000, provided by N.M.K. The following day, blots were labeled with secondary antibodies conjugated to horseradish peroxidase (HRP), (donkey) anti-mouse-HRP (Jackson ImmunoResearch). Stained gels and blots were imaged using a Bio-Rad ChemiDoc XRS+ imager.

ELISAs were performed in nondenaturing conditions as previously described (8). The 50-μL capture antibodies in PBS were bound to high-binding 96-well EIA/RIA Assay Microplates (Corning) in PBS overnight at 4 °C: (mouse) anti-TOC1 (20 ng/μL), (mouse) anti-TNT1 (20 ng/μL), (rabbit) anti-TauC4 (5 ng/μL; Sigma), or (mouse) anti-tau5 total tau (20 ng/μL). Wells were washed three times with 200 μL PBS, blocked with 5% nonfat dry milk in PBS (1 h at RT), and washed three times in PBS. Samples of reacted tau (diluted to 100 nM in 50 μL PBS) were incubated in wells for 2 h at RT, and then washed three times in PBS before addition of 50 μL detection antibodies in PBS for 2 h at RT: (mouse) anti-tau13 total tau (1:5,000) or (rabbit) anti-R1 total tau (1:5,000). Plates were washed three times in PBS then incubated 2 h at RT in 50 μL PBS with HRP-conjugated (donkey) anti-rabbit IgG or (donkey) anti-mouse IgG (Jackson ImmunoResearch, 1:5,000). Plates were washed three times in PBS and incubated in *o*-phenylenediamine (OPD) solution (1 mg/mL in 50 mM sodium phosphate, pH 5.0, 50 mM citric acid, and 1% hydrogen peroxide) for 15 min at RT. Reactions were stopped using 2.5 M sulfuric acid, and the absorbance was measured at 490 nm by a SpectraMax i3× plate reader. Graphing and statistical comparisons were performed as indicated in GraphPad Prism.

Primary Neuronal Culture. All animals were housed and treated in accordance with Boston University institutional animal care and use committee protocols. Primary hippocampal neurons were isolated from P0 C57BL/6J pups and cultured similarly to our previous studies (25, 54) (*SI Appendix, Materials and Methods*). After 7 DIV, neurons were exposed to tau + TIA1 reacted samples (below) by careful removal of media and replacement with conditioned media into which treatments were diluted. Neurons were then cultured for a further 7 d (to DIV14) with replenishment of media every third day.

Recombinant protein species for treatments were made as follows: 1) Uninduced tau = 5 μM (200 ng/μL) 0N4R WT tau in 10 mM Hepes pH 7.4, 100 mM NaCl mixed and immediately snap frozen on dry ice; 2) uninduced TIA1 = 5 μM (166.5 ng/μL) HIS::TIA1 in 10 mM Hepes pH 7.4, 100 mM NaCl mixed and immediately snap frozen on dry ice; 3) liquid tau = 5 μM 0N4R WT tau in 10 mM Hepes pH 7.4, 100 mM NaCl, induced with 10% PEG and 20 ng/μL total murine brain RNA, incubated 2 h at RT then snap frozen on dry ice; 4)

vitrified tau = 5 μM 0N4R WT tau and 5 μM HIS::TIA1 in 10 mM Hepes pH 7.4, 100 mM NaCl, induced with 10% PEG and 20 ng/μL total murine brain RNA, incubated 2 h at RT then snap frozen on dry ice; 5) fibrillar tau = 5 μM 0N4R WT tau in 10 mM Hepes pH 7.4, 100 mM NaCl, 1 mM DTT induced with 20 ng/μL total murine brain RNA, incubated 6 h at 37 °C, then snap frozen on dry ice; and 6) oligomeric tau = 5 μM 0N4R WT tau and 5 μM HIS::TIA1 in 10 mM Hepes pH 7.4, 100 mM NaCl, 1 mM DTT induced with 20 ng/μL total murine brain RNA, incubated 6 h at 37 °C then snap frozen on dry ice. Where cells were treated with l.tau or f.tau, uninduced TIA1 was added to the conditioned treatment media (but not the l.tau or f.tau reactions) at equal concentrations; this controls for the presence of TIA1 in the v.tau or o.tau samples.

At completion of the experiment (DIV14), culture media were collected for LDH cytotoxicity assay. LDH assay, CytoTox 96 (Promega), was performed according to manufacturer's protocol in a 96-well assay plate, read at 490-nm absorbance by a SpectraMax i3× plate reader. Fixed, permeabilized, and blocked neurons were immunolabeled with (chicken) anti-MAP2 (1:400, Aves) primary antibodies, then with (donkey) anti-chicken-AF647 (1:400, Jackson ImmunoResearch), then counterstained with DAPI (*SI Appendix, Materials and Methods*). Neurons were imaged at 20× on a Zeiss AxioObserver A1 epifluorescent microscope. The number of DAPI-stained nuclei within MAP2-positive cells was quantified using Imaris (BitPlane). Graphing and statistical comparisons were performed as indicated in GraphPad Prism.

Data Availability. All study data are included in the article and/or supporting information.

ACKNOWLEDGMENTS. We thank the following funding agencies for their support: NIH (AG050471, NS089544, AG056318, AG064932, and AG061706 to B.W.), the BrightFocus Foundation (B.W.), and NIH (GM126150 to P.I.).

1. D. M. Holtzman, J. C. Morris, A. M. Goate, Alzheimer's disease: The challenge of the second century. *Sci. Transl. Med.* **3**, 77sr1 (2011).
2. M. Goedert *et al*., Assembly of microtubule-associated protein tau into Alzheimer-like filaments induced by sulphated glycosaminoglycans. *Nature* **383**, 550–553 (1996).
3. M. E. King, T. C. Gamblin, J. Kuret, L. I. Binder, Differential assembly of human tau isoforms in the presence of arachidonic acid. *J. Neurochem.* **74**, 1749–1757 (2000).
4. T. Kampers, P. Friedhoff, J. Biernat, E. M. Mandelkow, E. Mandelkow, RNA stimulates aggregation of microtubule-associated protein tau into Alzheimer-like paired helical filaments. *FEBS Lett.* **399**, 344–349 (1996).
5. X. Wang *et al*., The proline-rich domain and the microtubule binding domain of protein tau acting as RNA binding domains. *Protein Pept. Lett.* **13**, 679–685 (2006).
6. J. E. Gerson, D. L. Castillo-Carranza, R. Kayed, Advances in therapeutics for neurodegenerative tauopathies: Moving toward the specific targeting of the most toxic tau species. *ACS Chem. Neurosci.* **5**, 752–769 (2014).
7. S. S. Shafiei, M. J. Guerrero-Muñoz, D. L. Castillo-Carranza, Tau oligomers: Cytotoxicity, propagation, and mitochondrial damage. *Front. Aging Neurosci.* **9**, 83 (2017).
8. D. J. Apicco *et al*., Reducing the RNA binding protein TIA1 protects against tau-mediated neurodegeneration in vivo. *Nat. Neurosci.* **21**, 72–80 (2018).
9. L. Jiang *et al*., TIA1 regulates the generation and response to toxic tau oligomers. *Acta Neuropathol.* **137**, 259–277 (2019).
10. C. A. Lasagna-Reeves *et al*., Tau oligomers impair memory and induce synaptic and mitochondrial dysfunction in wild-type mice. *Mol. Neurodegener.* **6**, 39 (2011).
11. C. A. Lasagna-Reeves *et al*., Alzheimer brain-derived tau oligomers propagate pathology from endogenous tau. *Sci. Rep.* **2**, 700 (2012).
12. S. Maeda *et al*., Granular tau oligomers as intermediates of tau filaments. *Biochemistry* **46**, 3856–3861 (2007).
13. S. Xu, K. R. Brunden, J. Q. Trojanowski, V. M. Y. Lee, Characterization of tau fibrillization in vitro. *Alzheimers Dement.* **6**, 110–117 (2010).
14. D. M. Mitrea, R. W. Kriwacki, Phase separation in biology; functional organization of a higher order. *Cell Commun. Signal.* **14**, 1 (2016).
15. Y. Shin, C. P. Brangwynne, Liquid phase condensation in cell physiology and disease. *Science* **357**, eaaf4382 (2017).
16. A. Hernández-Vega *et al*., Local nucleation of microtubule bundles through tubulin concentration into a condensed tau phase. *Cell Rep.* **20**, 2304–2312 (2017).
17. P. E. Wright, H. J. Dyson, Intrinsically unstructured proteins: Re-assessing the protein structure-function paradigm. *J. Mol. Biol.* **293**, 321–331 (1999).
18. M. R. Jensen, M. Zweckstetter, J. Huang, M. Blackledge, Exploring free-energy landscapes of intrinsically disordered proteins at atomic resolution using NMR spectroscopy. *Chem. Rev.* **114**, 6632–6660 (2014).
19. S. Wegmann *et al*., Tau protein liquid-liquid phase separation can initiate tau aggregation. *EMBO J.* **37**, e98049 (2018).
20. X. Zhang *et al*., RNA stores tau reversibly in complex coacervates. *PLoS Biol.* **15**, e2002183 (2017).
21. Y. Lin *et al*., Narrow equilibrium window for complex coacervation of tau and RNA under cellular conditions. *eLife* **8**, e42571 (2019).
22. T. Vanderweyde *et al*., Contrasting pathology of the stress granule proteins TIA-1 and G3BP in tauopathies. *J. Neurosci.* **32**, 8270–8283 (2012).
23. J. M. Silva *et al*., Dysregulation of autophagy and stress granule-related proteins in stress-driven Tau pathology. *Cell Death Differ.* **26**, 1411–1427 (2019).
24. N. M. Kanaan, C. Hamel, T. Grabinski, B. Combs, Liquid-liquid phase separation induces pathogenic tau conformations in vitro. *Nat. Commun.* **11**, 2809 (2020).
25. T. Vanderweyde *et al*., Interaction of tau with the RNA-binding protein TIA1 regulates tau pathophysiology and toxicity. *Cell Rep.* **15**, 1455–1466 (2016).
26. B. F. Maziuk *et al*., RNA binding proteins co-localize with small tau inclusions in tauopathy. *Acta Neuropathol. Commun.* **6**, 71 (2018).
27. N. Gilks *et al*., Stress granule assembly is mediated by prion-like aggregation of TIA-1. *Mol. Biol. Cell* **15**, 5383–5398 (2004).
28. J. Wang *et al*., A molecular grammar governing the driving forces for phase separation of prion-like RNA binding proteins. *Cell* **174**, 688–699.e16 (2018).
29. D. W. Sanders *et al*., Competing protein-RNA interaction networks control multiphase intracellular organization. *Cell* **181**, 306–324.e28 (2020).
30. T. Ukmar-Godec, S. Wegmann, M. Zweckstetter, Biomolecular condensation of the microtubule-associated protein tau. *Semin. Cell Dev. Biol.* **99**, 202–214 (2019).
31. P. J. Flory, Thermodynamics of high polymer solutions. *J. Chem. Phys.* **10**, 51–61 (1942).
32. R. J. Ellis, Macromolecular crowding: Obvious but underappreciated. *Trends Biochem. Sci.* **26**, 597–604 (2001).
33. J. B. Bryan, B. W. Nagle, K. H. Doenges, Inhibition of tubulin assembly by RNA and other polyanions: Evidence for a required protein. *Proc. Natl. Acad. Sci. U.S.A.* **72**, 3570–3574 (1975).
34. M. M. Emara *et al*., Angiogenin-induced tRNA-derived stress-induced RNAs promote stress-induced stress granule assembly. *J. Biol. Chem.* **285**, 10959–10968 (2010).
35. J. Cao, D. B. Cowan, D. Z. Wang, tRNA-derived small RNAs and their potential roles in cardiac hypertrophy. *Front. Pharmacol.* **11**, 572941 (2020).
36. S. M. Lyons, C. Achorn, N. L. Kedersha, P. J. Anderson, P. Ivanov, YB-1 regulates tiRNA-induced Stress Granule formation but not translational repression. *Nucleic Acids Res.* **44**, 6949–6960 (2016).
37. P. Ivanov, M. M. Emara, J. Villen, S. P. Gygi, P. Anderson, Angiogenin-induced tRNA fragments inhibit translation initiation. *Mol. Cell* **43**, 613–623 (2011).
38. M. Zuker, Mfold web server for nucleic acid folding and hybridization prediction. *Nucleic Acids Res.* **31**, 3406–3415 (2003).
39. A. Molliex *et al*., Phase separation by low complexity domains promotes stress granule assembly and drives pathological fibrillization. *Cell* **163**, 123–133 (2015).
40. N. L. Kedersha, M. Gupta, W. Li, I. Miller, P. Anderson, RNA-binding proteins TIA-1 and TIAR link the phosphorylation of eIF-2 alpha to the assembly of mammalian stress granules. *J. Cell Biol.* **147**, 1431–1442 (1999).
41. M. Feric *et al*., Coexisting liquid phases underlie nucleolar subcompartments. *Cell* **165**, 1686–1697 (2016).
42. S. Maharana *et al*., RNA buffers the phase separation behavior of prion-like RNA binding proteins. *Science* **360**, 918–921 (2018).
43. K. Santacruz *et al*., Tau suppression in a neurodegenerative mouse model improves memory function. *Science* **309**, 476–481 (2005).
44. A. B. Rocher *et al*., Structural and functional changes in tau mutant mice neurons are not linked to the presence of NFTs. *Exp. Neurol.* **223**, 385–393 (2010).
45. J. L. Crimins, A. B. Rocher, J. I. Luebke, Electrophysiological changes precede morphological changes to frontal cortical pyramidal neurons in the rTg4510 mouse model of progressive tauopathy. *Acta Neuropathol.* **124**, 777–795 (2012).
46. S. Maeda *et al*., Increased levels of granular tau oligomers: An early sign of brain aging and Alzheimer's disease. *Neurosci. Res.* **54**, 197–201 (2006).
47. H. C. Tai *et al*., The synaptic accumulation of hyperphosphorylated tau oligomers in Alzheimer disease is associated with dysfunction of the ubiquitin-proteasome system. *Am. J. Pathol.* **181**, 1426–1435 (2012).
48. Z. Berger *et al*., Accumulation of pathological tau species and memory loss in a conditional model of tauopathy. *J. Neurosci.* **27**, 3650–3662 (2007).
49. K. R. Patterson *et al*., Characterization of prefibrillar Tau oligomers in vitro and in Alzheimer disease. *J. Biol. Chem.* **286**, 23063–23076 (2011).
50. N. M. Kanaan *et al*., Pathogenic forms of tau inhibit kinesin-dependent axonal transport through a mechanism involving activation of axonal phosphotransferases. *J. Neurosci.* **31**, 9858–9868 (2011).
51. W.-C. Tsai *et al*., Arginine demethylation of G3BP1 promotes stress granule assembly. *J. Biol. Chem.* **291**, 22671–22685 (2016).
52. S. Guil, J. C. Long, J. F. Cáceres, hnRNP A1 relocalization to the stress granules reflects a role in the stress response. *Mol. Cell. Biol.* **26**, 5744–5758 (2006).
53. Y. Lin, D. S. W. Protter, M. K. Rosen, R. Parker, Formation and maturation of phase-separated liquid droplets by RNA-binding proteins. *Mol. Cell* **60**, 208–219 (2015).
54. L. Jiang, J. Zhao, J.-X. Cheng, B. Wolozin, Tau oligomers and fibrils exhibit differential patterns of seeding and association with RNA binding proteins. *Front. Neurol.* **11**, 579434 (2020).
55. J. N. Rauch *et al*., LRP1 is a master regulator of tau uptake and spread. *Nature* **580**, 381–385 (2020).
56. B. B. Holmes *et al*., Proteopathic tau seeding predicts tauopathy in vivo. *Proc. Natl. Acad. Sci. U.S.A.* **111**, E4376–E4385 (2014).
57. C. A. Lasagna-Reeves *et al*., Identification of oligomers at early stages of tau aggregation in Alzheimer's disease. *FASEB J.* **26**, 1946–1959 (2012).
58. S. L. DeVos *et al*., Synaptic tau seeding precedes tau pathology in human Alzheimer's disease brain. *Front. Neurosci.* **12**, 267 (2018).

59. M. L. Frandemiche *et al*., Activity-dependent tau protein translocation to excitatory synapse is disrupted by exposure to amyloid-beta oligomers. *J. Neurosci.* **34**, 6084–6097 (2014).
60. S. Markmiller *et al*., Context-dependent and disease-specific diversity in protein interactions within stress granules. *Cell* **172**, 590–604.e13 (2018).
61. J. B. Rayman, K. A. Karl, E. R. Kandel, TIA-1 self-multimerization, phase separation, and recruitment into stress granules are dynamically regulated by Zn^2. *Cell Rep.* **22**, 59–71 (2018).
62. I. R. Mackenzie *et al*., TIA1 mutations in amyotrophic lateral sclerosis and frontotemporal dementia promote phase separation and alter stress granule dynamics. *Neuron* **95**, 808–816.e9 (2017).
63. D. W. Cleveland, S. Y. Hwo, M. W. Kirschner, Purification of tau, a microtubule-associated protein that induces assembly of microtubules from purified tubulin. *J. Mol. Biol.* **116**, 207–225 (1977).
64. E. M. Mandelkow, E. Mandelkow, Biochemistry and cell biology of Tau protein in neurofibrillary degeneration. *Cold Spring Harb. Perspect. Biol.* **3**, 1–25 (2011).
65. A. C. Alonso, I. Grundke-Iqbal, K. Iqbal, K. Iqbal, Alzheimer's disease hyperphosphorylated tau sequesters normal tau into tangles of filaments and disassembles microtubules. *Nat. Med.* **2**, 783–787 (1996).
66. S. Khatoon, I. Grundke-Iqbal, K. Iqbal, Brain levels of microtubule-associated protein τ are elevated in Alzheimer's disease: A radioimmuno-slot-blot assay for nanograms of the protein. *J. Neurochem.* **59**, 750–753 (1992).
67. J. L. Guo, V. M. Y. Lee, Neurofibrillary tangle-like tau pathology induced by synthetic tau fibrils in primary neurons over-expressing mutant tau. *FEBS Lett.* **587**, 717–723 (2013).
68. Y. Shin *et al*., Spatiotemporal control of intracellular phase transitions using light-activated optoDroplets. *Cell* **168**, 159–171.e14 (2017).
69. C. Cook *et al*., Acetylation of the KXGS motifs in tau is a critical determinant in modulation of tau aggregation and clearance. *Hum. Mol. Genet.* **23**, 104–116 (2014).